Applied Catalysis A, General 629 (2022) 118423

Contents lists available at ScienceDirect

Applied Catalysis A, General

journal homepage: www.elsevier.com/locate/apcata

Fischer-Tropsch synthesis: Towards a highly-selective catalyst by lanthanide promotion under relevant CO_2 syngas mixtures

Jordi Guilera [a], José Antonio Díaz-López [b,*], Antonio Berenguer [a], Martí Biset-Peiró [a], Teresa Andreu [c]

[a] Catalonia Institute for Energy Research (IREC), Jardins de les Dones de Negre 1, 08930 Sant Adrià de Besòs, Spain
[b] Department of Mechanical, Chemical and Industrial Design Engineering, ETSIDI, Universidad Politécnica de Madrid (UPM), 28012 Madrid, Spain
[c] Departament de Ciència de Materials i Química Física, Universitat de Barcelona (UB), Martí i Franquès, 1, Barcelona 08028, Spain

ARTICLE INFO

Keywords:
Synthetic liquid fuels
Fischer-Tropsch synthesis, Carbon dioxide
Syngas
Reaction mechanism
Cobalt

ABSTRACT

The role of lanthanides as promoters on cobalt-based catalysts for Fischer-Tropsch synthesis was evaluated under relevant biomass-derived syngas mixtures. Cerium, lanthanum and a combination of them were impregnated on an industrial cobalt-based micro-catalyst. Lanthanide incorporation did not affect significantly the morphology of the catalyst, although it reduced the available surface cobalt. Catalytic tests revealed that both the presence of carbon dioxide in the feed and lanthanides in the catalyst led to similar outcomes; higher selectivity to long-chain hydrocarbons, at the expense of reactivity. Reaction experiments were well aligned with in-situ DRIFTS measurements, which evidenced the modification of the initial reaction mechanism, CO_2 conversion and the presence of lower CO-cobalt coverages. This work reports two relevant findings for FTS development. Firstly, the presence of carbon dioxide is beneficial for long-chain hydrocarbon production. Secondly, the incorporation of lanthanides increases the production of gasoline, kerosene and diesel fractions.

1. Introduction

Fischer-Tropsch synthesis (FTS) is a heterogeneously catalyzed reaction that turns syngas (CO and H_2) into a wide variety of hydrocarbons, from methane to long-chain products (> 100 carbon atoms). Therefore, it is possible to obtain transportation fuels (C_5-C_{20}) from alternative sources, which are of special interest for the harder-to-abate sectors: aviation, heavy-duty and shipping [1]. FTS is the core of the so-called X-To-Liquid routes; namely Gas-to-Liquid (GtL), Biomass-to-Liquid (BtL) and the more recent Power-to-Liquid (PtL) routes [2,3].

The interest in FTS has been renewed because of the development of BtL, through which it is possible to obtain liquid fuels from biomass-derived syngas [4]. This hydrogen-rich biosyngas can be composed of 50–52% hydrogen (H_2), 25–28% carbon monoxide (CO), 16–19% carbon dioxide (CO_2), 4–6% methane (CH_4) and traces of sulfur dioxide (H_2S) [5,6]. In other gasification approaches, lower H_2/CO are expected and feeding additional hydrogen to the biosyngas would be necessary [7,8]. Besides, utilizing CO_2 from industrial processes, biogenic sources or directly from air to produce synthetic fuels by PtL routes has gained much attention in recent years [9]. As the input of FTS is syngas, CO_2 can be converted in a preliminary unit by reverse water gas shift reactors or using solid oxide electrolysis cells [10]. In both cases, some CO_2 is still present in the outlet syngas due to kinetic and equilibrium constraints [11,12]. Therefore, the presence of CO_2 cannot be ignored in FTS, regardless the renewable origin of syngas (BtL or PtL).

Although CO_2 removal from syngas is technically feasible by membrane separation [13] or by classical amine absorption units [14], it would lead to a critical increase of feedstock cost, reducing the competitiveness of the whole process [4]. In this regard, research efforts have been made to understand how the presence of CO_2 affects the FTS process. Park et al. [15] reported a slightly faster deactivation and higher CH_4 formation under CO_2-rich environment (20% CO_2 in syngas) using cobalt-based catalysts. In addition, a decrease of catalytic activity and C_{5+} selectivity was observed, in agreement with those reported previously by Kim et al. [16], which were related to partial surface

Abbreviations: FTS, Fischer-Tropsch synthesis; GtL, Gas-to-Liquid; BtL, Biomass-to-Liquid; PtL, Power-to-Liquid; XRD, X-ray Diffraction; FWHM, full width of the diffraction line at half maximum; H_2-TPR, temperature programmed reduction; DRIFTS, Diffuse reflectance infrared Fourier transform spectroscopy; μGC, gas microchromatograph; rWGS, reverse Water Gas Shift.

* Corresponding author.
E-mail address: jose.dlopez@upm.es (J.A. Díaz-López).

https://doi.org/10.1016/j.apcata.2021.118423
Received 3 August 2021; Received in revised form 29 October 2021; Accepted 29 October 2021
Available online 3 November 2021

oxidation of metal active sites by CO_2. A negative effect was also reported by Díaz et al. [17], which was attributed to the fact that CO and CO_2 competed to be adsorbed on the same active sites.

Conversely, Kaiser et al. stated that CO_2 in FTS has no influence on CO conversion and product selectivity [18]. A subsequent kinetic study confirmed the negligible or minor influence of CO_2 on the reaction rates using a commercial cobalt catalyst [19]. At the other end, Yao et al. reported a positive effect because CO_2 can be converted to hydrocarbon products [20]. They suggested that CO_2 hydrogenation occurs through the formation of CO as intermediate. Analogously, Riedel et al. proposed a kinetic mechanism for the two-step reaction, in which CO formation is limited by equilibrium [21]. Kim et al. found that the addition of CO_2 increased C_{5+} selectivity [22]. On the whole, the relationship between the presence of CO_2 and the FTS performance seems complex as several intrinsic reaction mechanisms on catalytic active sites are involved.

Ruthenium, nickel, iron and cobalt are the active metals most often used in FTS. Cobalt seems the most active, stable and selective active metal to long-chain paraffinic hydrocarbons [23]. Even so, catalyst deactivation and selectivity are major issues concerning FTS catalysts, including cobalt-based catalysts [24]. The incorporation of promoters such as noble metal or oxides have been demonstrated to modify the stability [25] or selectivity towards desired products [26]. In this sense, noble metals have been widely studied as promoters for cobalt-based FTS catalysts, such as Pt [25], Ru [27] or Rh [28], whereas lanthanide promoters, such as lanthanum (La) or cerium (Ce) oxides, have been seldom studied.

Concerning La, Iqbal et al. [29] synthesized La-promoted $CoMnO_x$ catalysts with different La loadings. All promoted catalysts showed lower CO conversion, but those with lower loadings of La (0.05 and 1 wt %) were less selective to undesired CH_4 and CO_2 and more selective to hydrocarbons. Zeng et al. [30] came previously to the same conclusion, either using La-promoted and Ce-promoted cobalt catalysts. In the case of Ce, Pardo-Tarifa et al. [31] prepared cobalt catalysts supported on Ce-Al_2O_3 supports for FTS. Their results showed that the presence of CeO_2 on the surface of the support favors the reducibility of cobalt oxides, which led to an increase in catalytic activity and selectivity to long-chain hydrocarbons. Finally, He et al. [32] evaluated the effect of La and Ce as promoters of Co/SiO_2 catalyst. They inferred synergetic effect of co-promoted catalyst with an appropriate molar ratio, in terms of CO conversion and products selectivity, compared to unpromoted or single-promoted catalysts.

Literature results agree on the positive role of La and Ce as promoters on the selectivity to long-chain hydrocarbons (C_{5+}), whereas their effect on the conversion level is not clear. Further work is required to understand the effect of lanthanide promoted catalyst on the FTS mechanism. In that sense, it is essential to obtain molecular-level information of the nature of the adsorbed species and their respective evolution during the FTS reaction, as well as to explore reactants, products and possible intermediates on lanthanide promoted cobalt catalysts. Moreover, the vast majority of studies on those catalysts were carried out using ideal mixtures of H_2 and CO, although the presence of CO_2 in the inlet seems inevitable in practical applications. In that point, there is no consensus about how the presence of CO_2 affects the FTS performance. Accordingly, a series of Ce- and La-promoted cobalt catalysts were synthesized and tested in FTS using industrially relevant H_2/CO/CO_2 mixtures, such as those obtained through biomass gasification.

2. Experimental

2.1. Promoted catalyst synthesis

A micro-catalyst (Co/γ-Al_2O_3, 16.3 wt%) supplied by Johnson Matthey was used as a reference. γ-Al_2O_3 support, as 500 μm spheres, was also provided. Cerium (III) nitrate hexahydrate [$Ce(NO_3)_3.6H_2O$, 99.5%, Acros Organics] and lanthanum (III) nitrate hexahydrate [$La(NO_3)_3.6H_2O$, 99.9%, Merck] were used respectively as Ce and La precursors. Precursors of lanthanide metals were loaded into the reference catalyst by incipient wetness impregnation procedure [33]. First of all, 5 g of the reference catalyst (pore volume: 0.312 $cm^3\ g^{-1}$) were dried at 60 ºC under vacuum. At the same time, Ce, La or both precursors (Ce-La, Ce/La = 1 (molar)) were dissolved in the exactly amount of water to fill the catalyst pores. The total molar ratio promoters/cobalt was 0.1. After that, the aqueous solution was added dropwise over the raw materials. Then, samples were dried in a rotary evaporator under vacuum following this procedure, 75 ºC during 2 h and 90 ºC during the next 4 h. Afterwards, the impregnated materials were kept at 105 ºC in an atmospheric oven overnight, and subsequently, calcined at 350 ºC (heating rate: 2 ºC min^{-1}) for 2 h under static air conditions.

2.2. Characterization techniques

All samples were characterized by a series of techniques with the aim to correlate their structural and physicochemical properties and metal-support interactions with the activity results. Chemical composition of samples (Al, Co, La and Ce) was determined by inductively coupled plasma with atomic emission spectroscopy (ICP-AES) in an Optima Perkin Elmer 3200 RL apparatus.

Textural properties were determined from N_2-physisorption (adsorption/desorption) isotherms recorded by a TriStar II 3020-Micromeritics sorption analyzer. Structural properties were studied by powder X-ray Diffraction (XRD). The wide-angles data were obtained on a Bruker type XRD D8 Advance A25 diffractometer. The average crystal size was calculated using the Scherrer's equation: $dCo_3O_4 = (K\lambda/\beta Cos\Theta)$, where λ is the X-ray wavelength, β is the full width of the diffraction line at half maximum (FWHM), and Θ is the Bragg angle. Reducibility of the catalysts was analyzed by temperature programmed reduction method (H_2-TPR) on an Autochem 2890 (Micromeritics). Experimental procedures were previously reported [34,35].

The extent of cobalt reduction was studied using O_2 titration experiments, which were conducted in the same apparatus as used for the TPR experiments. Firstly, samples were reduced in a 50 NmL min^{-1} H_2 flow (12 vol% H_2/Ar) at 120 ºC during 2 h following by 380 ºC for 7 h. After reduction, sample was kept at 380 ºC in He and held for 1 h to desorb any chemisorbed H_2. Calibrated pulses of O_2 were then added into the continuous He flow until further consumption of O_2 was not detected by the TCD located downstream from the reactor. The extent of reduction was calculated assuming stoichiometric re-oxidation of Co^0 to Co_3O_4.

Metal surface area was determined by pulsed CO chemisorption in the same apparatus as used for the TPR and O_2 titration experiments. Prior to adsorption measurements, each sample (150 mg) was reduced in 50 NmL min^{-1} of H_2 flow (12 vol% H_2/Ar) at 120 ºC during 2 h following by 380 ºC for 7 h. Then, the system was cooled down to 35 ºC. CO uptake was measured by injecting CO pulses through a calibrated on-line sampling valve (0.5215 cm^3 10%CO/He) until saturation was attained. Cobalt dispersion was calculated assuming the stoichiometric factor for CO to cobalt as one and atomic weight of 58.93. It is important to point out that CO adsorption on cobalt is a complex process; the stoichiometry can vary with metal dispersion, metal loading, temperature, preparation method and it can form volatile complexes [23].

2.3. In situ DRIFTS experiments

In situ Diffuse Reflectance Infrared Fourier Transform Spectroscopy (DRIFTS), in which a special IR cell acts as a reactor, was used as a well-tested technique to obtain information about the adsorbed species and their evolution. DRIFTS experiments were performed at ambient pressure with a high temperature DRIFTS cell (from Harrick Scientific Corporation) fitted with ZnSe windows, using a collector assembly (Praying MantisTM). The spectrophotometer used was a Vertex 70 (Bruker) fitted with liquid N_2 cooled DigiTect MCT-detector. The DRIFTS spectra were recorded at a resolution of 4 cm^{-1} and 64 scans accumulation. The

sample hole of the cell was filled with 70–80 mg of catalyst spheres. Catalysts were in-situ reduced at 380 ºC for 1 h in a flow of 20 NmL min^{-1} of pure H_2.

DRIFTS analyzes were carried out at single FTS reaction temperature. Samples were cooled down to the reaction temperature of 230 ºC. After 30 min at 230 ºC in H_2 atmosphere, a spectrum was recorded and used as background for all the following spectra recorded along the reaction. Two feed composition were used: a) 50% of H_2/CO (H_2/CO ≈ 2.1 vol.) and 50% of Ar, and b) 50% of H_2/CO (H_2/CO ≈ 2.1 vol.), 32.5% of CO_2. and 17.5% of Ar. The system was always operated at ambient pressure and the total flow rate was 40 NmL min^{-1}. The reaction time was 4–24 h.

2.4. Catalytic tests

Fischer-Tropsch catalytic studies were carried out in a fixed-bed reactor (Microactivity Reference, PID Eng&Tech). H_2 (99.999%, Linde), CO (99.5%, Linde), CO_2 (99.9993%, Linde) and N_2 (99.999%, Linde) were used in each catalytic run. After reaction, the reactor effluent passed through two consecutive traps. In the first one (100 ºC and 20 barg), waxes were trapped together with some H_2O, whereas the second one (10 ºC and 20 barg), retained liquid hydrocarbons and remaining H_2O. The whole system (traps excluded) was placed in a hot box at 150 ºC to avoid possible condensations on the pipelines.

Experiments were conducted using 0.5 g of catalysts particles, sieved to 400–500 μm. Catalyst were diluted in 5 g of SiC 46 grit of similar particle size (355 μm) to minimize the temperature gradients throughout the catalytic bed (length about 5.2 cm). Prior to reaction, catalysts were reduced in-situ under 100 NmL min^{-1} of H_2 at 380 ºC and atmospheric pressure, with a hold time of 7 h and a heating ramp of 1 ºC min^{-1}. After reduction, the system was cooled down to 150 ºC under hydrogen atmosphere. Once the temperature was attained, 200 NmL min^{-1} of the reactant mixture was introduced and pressure was raised up to 20 barg. Nitrogen was used as internal standard. Three different reactant mixtures were used in this study: #1 syngas, 95% of H_2/CO (H_2/CO ≈ 2 vol.) and 5% N_2; #2 syngas diluted with N_2, 70% of H_2/CO (H_2/CO ≈ 2.1 vol.) and 30% N_2; and #3 syngas diluted with CO_2, 70% of H_2/CO (H_2/CO ≈ 2.1 vol.), 25% CO_2 and 5% N_2.

This condition was held for 6 h, during which the concentration of the reactant mixture was analysed and taken as a reference for activity and selectivity calculations. Afterwards, the temperature was raised to 230 ºC, keeping 200 NmL min^{-1} of reactant flow for 16 h. Finally, the GHSV was adjusted to get a CO conversion of approximately 50% (45–60%) to compare the catalyst selectivity at a similar level of conversion.

The gas effluent (light hydrocarbons, CO_2 and the remaining reactant mixture) was analysed online with a gas micro-chromatograph (μGC) equipped with a TCD (490 microGC, Agilent Technologies), which was previously calibrated using different cylinders and N_2 as standard. Liquid products and waxes were analysed by a Gas Chromatograph-Mass Spectrometer, GC-MS, Agilent technologies 7840 GC-5975C inter XL MSD (Electron energy 70 eV, Emission 929 V; Column DB-5MS (30 m x 0.25 mm ID x 0.25 μm). NIST EI-MS spectral library was used for compounds identification (with a minimum match score of 700). Hydrocarbons have been further divided in groups according to the number of carbon atoms in their chains.

The liquid products distribution of all promoted catalysts was also evaluated by the Anderson-Schulz-Flory (ASF) equation:

$$\frac{W_n}{n} = (1-\alpha)^2\alpha^{n-1} \quad (1)$$

where W_n is the mass fraction of a hydrocarbon with chain length n, and α is the chain growth probability. A plot of logarithm of W_n/n vs n would produce a straight line plot whose slope is related to α. ASF equation was applied using W_n results of paraffin in the range C_6-C_{34}.

3. Results and discussion

3.1. Catalyst properties

A series of catalyst samples were prepared by incipient wetness impregnation of Ce, La and a combination of both, on an industrial cobalt-based micro-catalyst. The properties of the samples are presented and discussed in this section. Table 1 lists the composition, surface area, pore volume and average pore diameter. The chemical composition determined by ICP-AES was in agreement with the expected nominal values. Samples were composed a fixed cobalt content of 14–16 wt%. Promoted samples incorporated 3.18–3.30 wt% of lanthanides, either in the form of cerium, lanthanum or a combination of both; which is equivalent to the molar ratio promoter/cobalt of 0.09–0.10. Surface area decreased significantly with the incorporation of cobalt on the support (− 25%), whereas promoted samples presented similar surface area. Instead, pore volume of promoted catalysts was higher than that of the reference, which can be related to promoter deposition on larger support pores.

Fig. 1 shows the nitrogen adsorption-desorption isotherms and the pore diameter distribution of the support – γ-Al_2O_3 – and the catalysts evaluated in the present work. All samples showed a mesoporous-type isotherm, without noticeable nitrogen adsorption in the micropore range. On the one hand, it is observed that the incorporation of lanthanides on reference did not cause any change in isotherm pattern, although an increase of N_2 adsorbed volume was observed at high relative pressure (0.5–1). On the other hand, the mesopore size distribution of lanthanide promoted catalysts slightly shifted to lower values than those of reference. This fact is a direct consequence of the promoter incorporation, which reduced the dimensions of the largest pores. Besides, it is noteworthy that there were no differences between promoted catalysts, so that La, Ce or the combination of them led to identical textural properties.

XRD patterns of all samples are depicted in Fig. 2. All catalysts showed a main narrow diffraction peak, identified as the crystalline phase Co_3O_4, at 36.84º (ICDD Card No. 00-042-1467). Small peaks of this crystalline phase, at ca. 31.32º, 45.08º, 59.58º and 65.44º, were also detected. Diffractograms of all catalysts were practically identical to each other, which revealed that dispersion of cobalt oxides was not strongly modified after promoter incorporation. Cobalt particle size, which was estimated using Scherrer Equation, was practically identical to each other (11.0–11.3 nm). Lastly, there were no diffraction peaks associated to CeO_2 or La_2O_3. In this sense, the most plausible explanation is that CeO_2 or La_2O_3 crystals were quite finely dispersed on the alumina surface below the typical detection limit of XRD of 1 vol%, to the point that they could not be detected by XRD [36].

TPR profiles are depicted in Fig. 3. In general, two main peaks were observed in all samples. All promoted materials exhibited a reduction

Table 1
Catalyst properties.

Sample	support	reference	Ce	La	CeLa
Co (wt%)[a]	–	15.51	14.84	14.21	15.10
Ce (wt%)[a]	–	nd	3.18	nd	1.59
La (wt%)[a]	–	nd	nd	3.30	1.62
surface area (m^2 g^{-1})	216	163	159	157	161
pore volume (cm^3 g^{-1})	0.492	0.312	0.379	0.374	0.370
pore diameter (nm)	9.06	8.54	8.39	8.33	8.30
Co_3O_4 particle size[b] (nm)	–	11.3	11.0	10.6	11.6
Co^0 particle size[b] (nm)	–	9.2	9.1	9.0	8.8
metal reduction (%)[c]	–	57.1	37.2	37.6	40.3
CO adsorption (cm^3 g^{-1})[d]	–	1.453	0.741	0.616	0.635
metal surface area (m^2 g^{-1})	–	2.58	1.32	1.10	1.13

[a] ICP.
[b] XRD.
[c] O_2 titration.
[d] CO chemisorption.

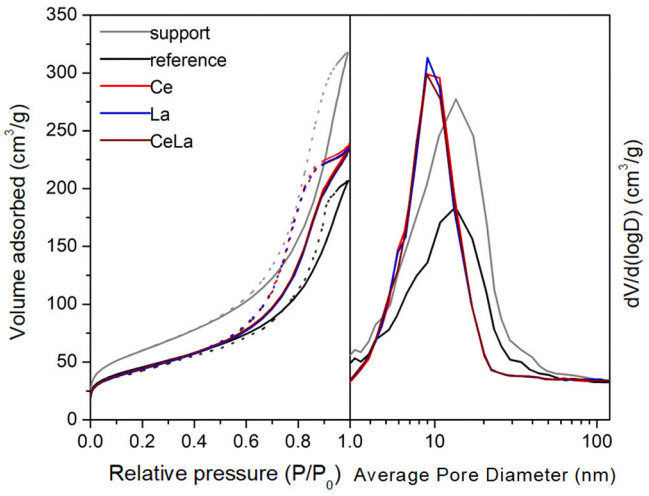

Fig. 1. N_2 adsorption-desorption isotherms at 77 K (left) and pore diameter distribution (right) of the support and the catalysts. Dashed lines represent desorption branches.

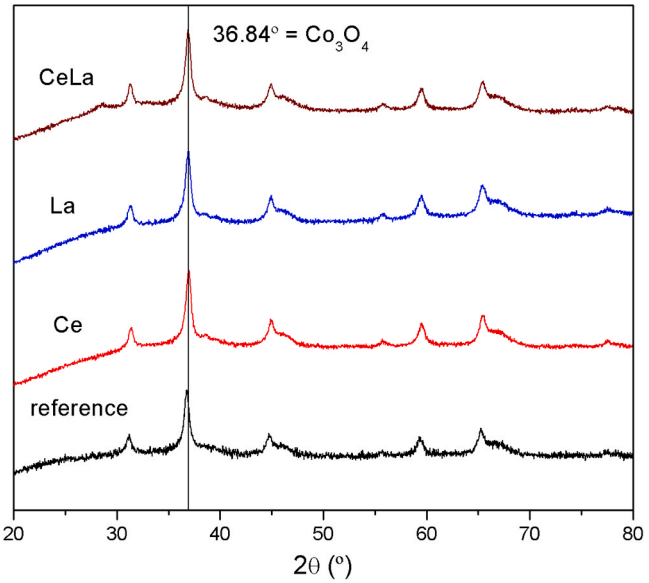

Fig. 2. XRD diffractograms of the catalysts used in this work prior to reduction.

pattern similar to that of the reference catalyst, with a first peak in the range 260–330 °C associated to the low temperature reduction of Co_3O_4 to CoO, and a second one, in the range 470–565 °C, which corresponds to the high temperature reduction of CoO to Co° [23,37]. However, it is important to underline three facts. Firstly, the intensity of the small shoulder (200–210 °C) observed in reference, which is associated with the decomposition of the residual nitrate salt precursor to NO_x [38], decreased after rare earth incorporation. This fact is associated with the calcination step, after the incorporation of promoters. Secondly, lanthanide promotion clearly shifted the TPR peaks associated to Co_3O_4 reduction to higher temperatures. These results suggested a stronger cobalt-support interaction in presence of lanthanides, especially Ce, which would hinder the reduction of cobalt particles [39]. Lastly, promoted samples showed a small shoulder (600–632 °C) which is accepted to be caused by the formation of irreducible species (cobalt aluminates) that are hard to reduce [40]. This event would support the hypothesis of the stronger cobalt-support interaction above mentioned. In any case, the selected reduction procedure at 380 °C leads to identical consequences in all samples, that is, complete reduction of Co_3O_4 to CoO and

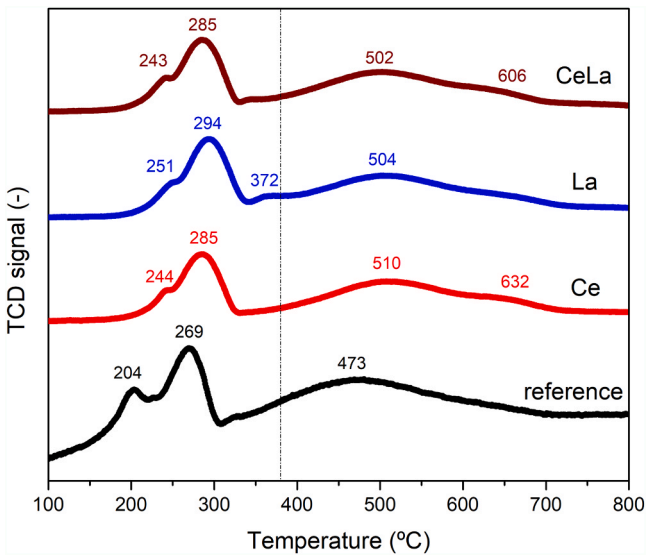

Fig. 3. TPR profiles of the catalysts used in this work. Dashed line indicates the reduction temperature selected.

the occurrence of CoO reduction to Co^0 at low reaction rate, but avoiding the formation of cobalt aluminates. Last but not least, it is important to note that unpromoted and promoted samples showed similar TPR profiles, so there was no noticeable reduction event associated to promoters.

TPR profiles shed light about reduction behavior, but are not enough to draw quantitative conclusions. In this sense, the extent of cobalt reduction was complementary evaluated by O_2 titration. As presented in Table 1, promoted samples exhibited lower percentage of reduced cobalt (37–40%) than the reference (57%). Therefore, both H_2-TPR and O_2 titration measurements indicate that cobalt particles are more difficult to reduce after lanthanide loading. Similar results were found by Carrero et al., which suggested that loading Ce and/or La in the samples makes cobalt-alumina interaction stronger [41]. Lu et al. proposed that some La mixed species can cover free surface metal species [42]. This is consistent with the metal surface area determined by pulsed CO chemisorption measurements after reduction at 380 °C under diluted H_2. In this direction, significantly lower metal surface area was observed on promoted samples (1.10–1.32 $m^2\ g^{-1}$) with respect to the reference (2.58 $m^2\ g^{-1}$). The lower metal surface area of promoted catalysts is attributed to active site coverage by lanthanide promoters, in addition to lower reduction levels of promoted samples under those conditions. In this aspect, addition of promoters before or during cobalt impregnation can be a promising route for future studies.

Fig. 4 depicts the XRD diffractograms of the catalysts after reduction. Besides the Co_3O_4 peaks above mentioned, a new one at ca. 42.7° appeared in all samples, which can be ascribed to metallic cobalt (ICDD Card No. 00-015-0806). Results confirmed, on the one hand, that the active phase was not completely reduced in all samples, as peaks associated to Co_3O_4 are still visible. On the other hand, small differences between cobalt particle size (8.8–9.2) were again observed. Nevertheless, it is observed that particle size of promoted catalysts were smaller than that of REF, which suggested that promoters favored slightly cobalt dispersion. In any case, cobalt sintering during reduction can be ruled out.

In summary, the incorporation of lanthanides to the reference catalyst i) slightly reduced the pore diameter, while increased the pore volume, ii) did not modify the cobalt particle size, iii) decreased the reducibility of cobalt and iv) reduced the amount of cobalt on the surface. A meaningful finding is that there were no considerable differences between La, Ce or a combination of them, as they led to identical properties.

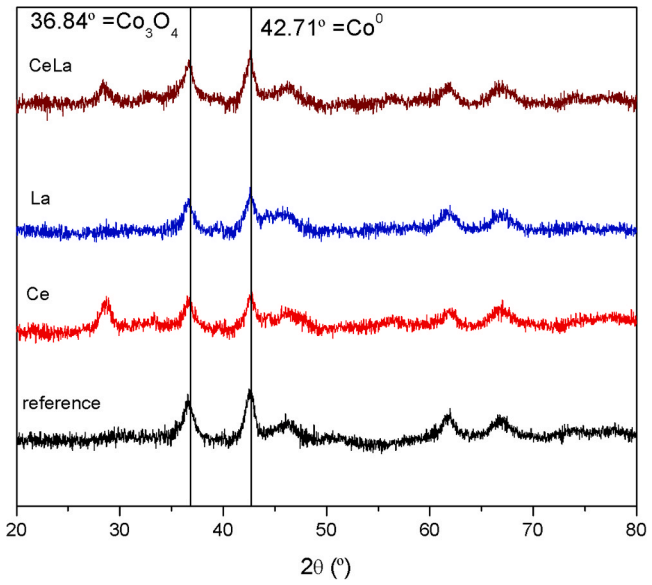

Fig. 4. XRD diffractograms of the catalysts used in this work after reduction.

3.2. Catalytic tests

3.2.1. Influence of CO_2 on the feed

A series of preliminary experiments were performed on the reference catalyst with the aim of evaluating how the presence of CO_2 affects FTS catalytic performance. GHSV was adjusted to get a similar conversion level. The maximum relative error observed between experimental species concentrations at equivalent time-on-stream (TOS) was less than 2%. Experimental results under different feed composition at similar level of conversion are listed in Table 2, which should be analysed through pairwise comparison.

First of all, the highest catalytic activity was found using syngas at the inlet (#1), namely H_2 and CO (5% N_2 as internal standard). Selectivity to CO_2 was kept below 1%. When other compound was introduced to the gas feed, either N_2 (#2) or CO_2 (#3), the catalytic activity decreased, as a notorious reduction of the GHSV values (− 56 and − 35%, respectively) was required to obtain similar CO conversion in both cases. These results supported the expected positive effect of reactant concentration on FTS kinetics, and therefore on reactant conversion. More relevant was the positive effect of CO_2 on the feedstream, when compared to N_2. As it can be observed, higher GHSV was used in experiment #3 than that of experiment #2 to get similar CO and H_2 conversion. Therefore, N_2 acted as a completely inert compound, while CO_2 played a role in the reaction. Remarkably, CO_2 conversion attained 13% in experiment #3, which will be discussed together with complementary experiments. Therefore, the CO_2 role was inverted from a residual product (#1) to an important reactant (#2), as the equilibrium of the reverse Water Gas Shift reaction (rWGS) was shifted because of the higher partial pressure of CO_2 in the feedstream. This hypothesis is supported by the fact that the difference between CO and H_2 conversion in experiment #3 (5.8% at 40 h TOS) is higher than that of experiment #2 (4.3% at 40 h TOS), which was expected considering that H_2 in rWGS acts as reactant and CO as a product. These additional CO molecules formed during the reaction in the presence of CO_2 increased the overall conversion with respect to N_2 dilution.

Selectivity to long-chain hydrocarbons (C_{5+}) was higher using either syngas (#1) or diluted with CO_2 (#3). According to Schulz [43], higher CO partial pressure inhibits methane desorption and chain termination steps, which consequently lead to hydrocarbons of longer chains. The positive effect of CO partial pressure on FTS selectivity was also reported by other authors [3]. Unexpectedly, it was found that the negative effect of decreasing the partial pressure of reactants could be balanced by the presence of CO_2 in the inlet. The presence of CO_2 favoured the formation of long-chain hydrocarbons, at the expense of methane and C_2-C_4 fraction. As CO_2 was revealed to be a reactant instead of an inert species, the resulting carbon ratio was higher, which favoured the formation of hydrocarbons of longer chain [44].

Fig. 5 represents the production of C_{5+} compounds using the different feeds. The overall production after 40 h of experiment was always lower than the corresponding initial one, showing a slight deactivation of the catalyst. The effect of adding CO_2 in the gas mixture was very beneficial in terms of productivity of C_{5+} products. Therefore, experimental results suggest that it is preferable to keep CO_2 in the gas mixture and carry out the gas separation after FTS reactor. In conclusion, replacement of part of syngas by N_2 or CO_2 led to lower catalytic activity due to the decrease of the partial pressure of reactants. However, part of the CO_2 was able to react with H_2, leading to higher catalytic performance. In order to shed light on the specific role of CO_2 in the reference catalyst, in-situ DRIFTS experiments were carried out.

3.2.2. In-situ DRIFTS experiments – influence of CO_2 on the feed

The evolution of the adsorbed species for 24 h on the reference catalyst using #1 syngas at the FTS reaction temperature is shown in

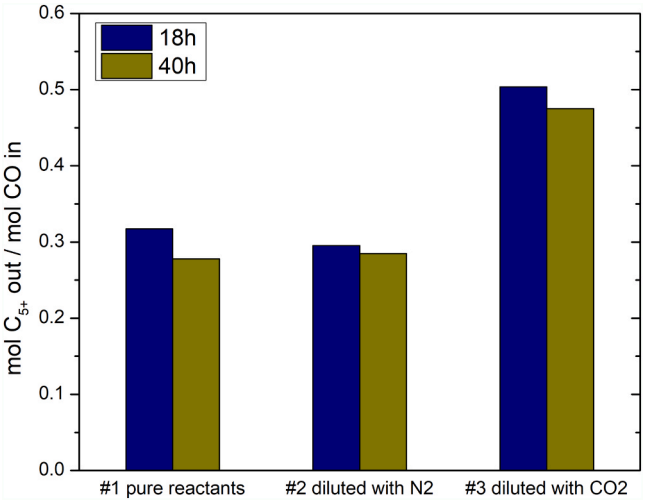

Fig. 5. Production of C_{5+} compounds per mole of CO using different feedstream composition.

Table 2
Catalytic results of the reference catalyst using different feed composition at 18 h and 40 h TOS. Reaction conditions: 20 bar, 230 ºC.

# experiment	Feed composition (vol.) $H_2/CO/CO_2/N_2$	GHSV (NmL h^{-1} g^{-1})	TOS (h)	Conversion (%)			Selectivity (%)		
				CO	H_2	CO_2	CH_4	C_2-C_4	C_{5+}
#1 syngas	63/32/0/5	8309	18	41.8	53.0	–	16.1	7.5	75.8
			40	38.1	49.9	–	15.4	11.1	73.0
#2 diluted with N_2	47/23/0/30	3618	18	55.4	59.9	–	19.2	15.8	63.6
			40	46.4	50.7	–	19.1	18.6	61.4
#3 diluted with CO_2	47/23/25/5	5406	18	52.4	58.3	13.1	15.2	8.7	76.1
			40	49.0	54.8	13.4	14.9	9.8	75.3

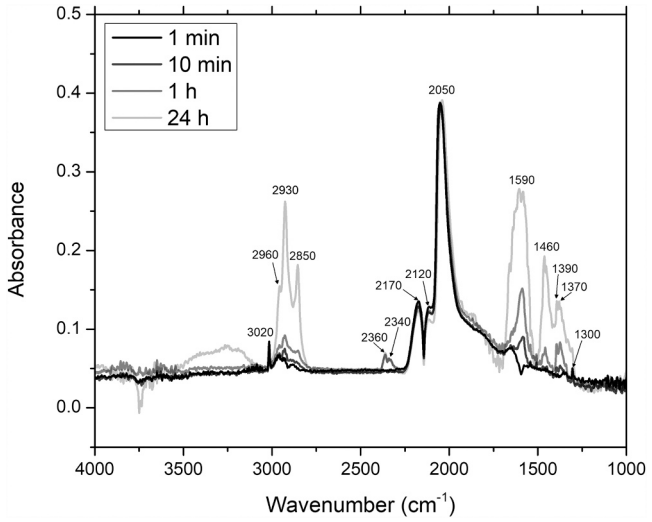

Fig. 6. DRIFTS experiments on reference catalyst over time catalyst using 50% H_2/CO – 50% Ar feed.

Fig. 6. For the sake of clarity, spectra at intermediate time was not shown. As a whole, the following 4 band groups were observed using CO and H_2: bands located at the oxygenate (1300–1590 cm^{-1}), CO (2050–2170 cm-1), CO_2 (2340–2360 cm^{-1}) and hydrocarbon (2850–3020 cm^{-1}) species region [45–47]. CO bands were observed from the very beginning of the experiment. CO_2 bands were also observed from the first minute, while oxygenate and hydrocarbon species increased progressively their presence until the end of the measurement at 24 h.

Fig. 7 presents the DRIFTS results including CO_2 in the reactant mixture. The pattern of most of the bands was quite similar, as CO and H_2 were still the majority compounds of the gas inlet, but some important differences were detected. As for the oxygenates region, bands associated to formate species (1600 cm^{-1}), C-H bending (1390 cm^{-1}), OCO stretching (1370 cm^{-1}), and bicarbonate (1230 cm^{-1}) were higher when CO_2 was present. These new or more intense adsorbed species suggest that CO_2 interacted with the alumina surface. This is in agreement with CO_2 adsorption on the support followed by reaction to form CO and carbonate species [48].

In comparison with CO_2-free measurements, the largest differences were i) huge increase of the CO_2-related signals (2350 cm^{-1}), either adsorbed or gas-phase band; and ii) the presence of a new group band, attributed to OH species region (3600–3730 cm^{-1}). In this region, the presence of adsorbed OH at 3630 cm^{-1} is assigned to adsorbed OH groups on Al_2O_3 [49]. This bands are also observed during the reverse Water Gas Shift reaction (rWGS) on Pt-based catalyst [48,50], where CO_2 is converted to CO. In particular, Lalinde et al. reported that the rate limiting step of rWGS corresponds to the formation of OH* on the catalyst surface [47] (Eq. 2). Thus, the conversion of CO_2 observed during catalytic runs can be attributed to the formation of CO by rWGS reaction. Analogous findings were observed at temperatures as low as 220 ºC using Fe catalyst [51]. In this aspect, when CO_2 was introduced in the feed, CO acted both as reactant and as intermediate to form FTS products.

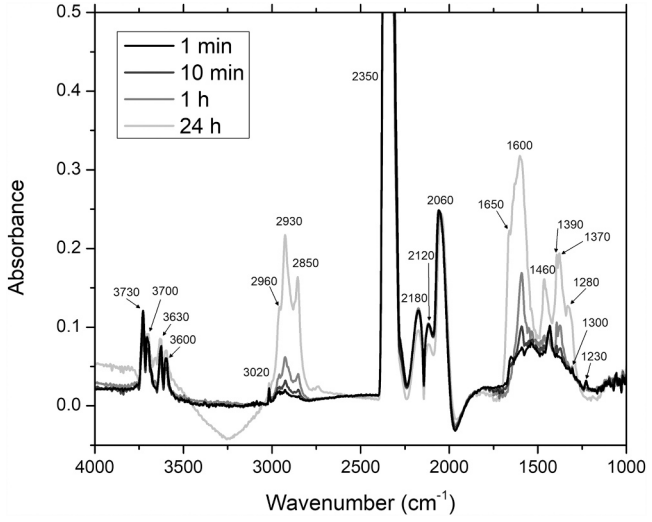

Fig. 7. DRIFTS experiments on reference catalyst over time catalyst using 50% H_2/CO – 32.5% CO_2 – 17.5% Ar feed.

$$CO_2^* + H^* \rightarrow CO^* + OH^* \quad (2)$$

Another important regard on CO_2 DRIFTS measurements, is the significantly decrease of the peak associated to CO linearly coordinated (2050–2060 cm^{-1}). Therefore, less amount of CO was adsorbed on cobalt nanoparticles during CO_2 runs. The competition of linearly adsorbed CO and CO_2 on active sites can explain the lower conversion observed in CO_2 catalytic runs. On the other hand, the band associated to formates and carboxylates (1460 cm^{-1}) shifted to C-H bending and OCO stretching (1370–1390 cm^{-1}) species, showing that the amount of reaction intermediates, and thus, the reaction mechanism was modified by the presence of CO_2. As for the hydrocarbon regions, the band attributed to the simplest hydrocarbon, CH_4 (3020 cm^{-1}), was less intense when CO_2 was part of the feedstream, whereas the other bands showed a similar behaviour. Therefore, product distribution was shifted to longer chain hydrocarbons, what can explain the highest selectivity to long-chain hydrocarbons in the catalytic runs.

In conclusion, DRIFTS results appear to be in line with catalytic experiments. The presence of CO_2 i) incorporates the rWGS reaction in the reaction mechanism, which is correlated with the presence of OH and carbonates, ii) modifies the absorbed species and inhibits the selectivity to shorter hydrocarbons and iii) reduces the amount of cobalt active sites for CO adsorption.

3.2.3. *Effect of lanthanide promotion*

In this section, the role of La and Ce as individual or combined promoters of the reference catalyst was studied on relevant H_2/CO/CO_2 mixtures. Experimental results at different reaction times are listed in Table 3. It can be inferred that promoted catalysts exhibited three main differences respect to reference. Firstly, i) all promoted catalysts were less active, which resulted in lower GHSV (− 30%) to achieve similar CO and H_2 conversion. Then, at similar CO conversion level ii) CO_2 conversion on promoted catalysts was much higher (+ 70%). Finally, iii) promoted catalysts were more selective to long-chain hydrocarbons (+ 11%).

Among lanthanide promoted samples, similar conversion and selectivity levels were observed, with minor differences between them. The C_{5+} selectivity value obtained with this catalyst was between those of Ce and La, whereas the syngas conversion was similar to that of La. It can be said that, using La and Ce as promoters simultaneously, it is possible to get a catalyst with similar properties as those obtained using one of these promoters, so substantial synergistic effects of combining La and Ce are discarded. Thus, the cost of raw materials can play a relevant role in the lanthanide promoter selection.

The lower reactivity of promoted catalysts can be linked with the lower availability of active cobalt sites on the surfaces, determined by CO chemisorption measurements. In this aspect, less amount of accessible cobalt nanoparticles was available in lanthanide promoted catalysts. In the case of higher CO_2 conversion and different products selectivity, additional in-situ DRIFTS measurements were carried out to elucidate if the reaction mechanism was modified by the presence of lanthanides.

Table 3
Catalytic results of lanthanide promoted catalysts at different TOS. Feed #3 diluted with CO_2. Reaction conditions: 20 bar, 230 °C.

Catalyst	GHSV (NmL h^{-1} g^{-1})	TOS (h)	Conversion (%)			Selectivity (%)			ASF-α
			CO	H_2	CO_2	CH_4	C_2-C_4	C_{5+}	
Reference	5406	18	52.4	58.3	13.1	15.2	8.7	76.1	0.8526
(#3Table 2)		40	49.0	54.8	13.4	14.9	9.8	75.3	
		74	46.8	52.3	6.4	16.7	11.6	71.7	
Ce	3718	19	54.0	64.3	20.3	10.5	5.3	84.3	0.8510
		45	50.6	55.2	17.3	13.7	4.4	81.9	
		119	45.3	49.0	14.5	8.7	8.3	83.0	
La	3702	19	61.5	66.7	21.9	9.7	5.5	84.8	0.8261
		41	55.4	60.4	20.6	9.7	8.0	82.3	
		115	52.9	57.9	15.9	10.6	9.1	80.3	
CeLa	3774	18	62.9	67.9	22.1	9.6	5.4	85.0	0.8349
		45	54.1	58.7	18.6	9.6	8.4	82.0	
		124	49.9	53.8	16.6	9.1	9.1	81.8	

Fig. 8 depicts the distribution of liquid and waxes products determined by GC-MS analysis, taking into consideration the selectivity to C_{5+} previously determined by micro gas-chromatography. The reference catalyst produced about 17% light compounds, 34% of diesel-type compounds, 25% of heavy products and some alcohols. Noticeably, lanthanide promoted samples produced a significantly + 17% higher amount of diesel-type compounds (C_{12}-C_{18}), + 10% higher amount of light compounds (C_5-C_{11}) and a similar amount of heavy compounds (C_{19}^+). Therefore, it can be concluded that lanthanide promotion of cobalt based catalyst favors the formation of C_5-C_{18} compounds. The differences in chain growth probability, obtained from Anderson-Schulz-Flory (ASF) Distribution, support this conclusion (see Table 3). The resulting liquid fuel feature characteristics that make them suitable substitutes for their fossil counterparts; namely gasoline, kerosene and diesel fuels.

3.2.4. *In-situ DRIFTS experiments – lanthanide promotion effect*

Fig. 9 shows the in-situ DRIFTS patterns of CeLa sample on #3 diluted with CO_2 mixture for 4 h, with the aim of elucidating the lanthanide promotion effect on the catalytic performance on relevant mixtures. At first sight, DRIFTS pattern of the lanthanide promoted sample was very similar as that of the reference. However, interesting divergences can be drawn. The area of the band associated with the presence of CO linearly bonded with cobalt metal active sites (2060 cm^{-1}) was smaller in CeLa, denoting lower cobalt coverages, in agreement with CO chemisorption technique. According to these observations, the lower conversion of CeLa respect to reference may be related to the lower coverage of metallic cobalt particles, which could be limiting the use of CO to start the formation of hydrocarbons.

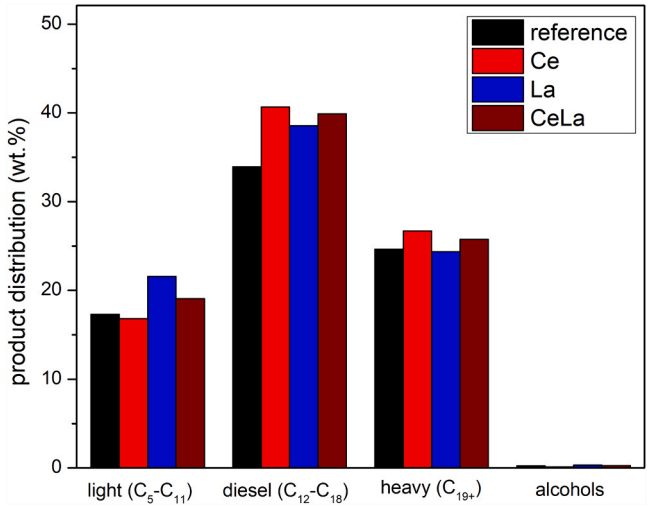

Fig. 8. C_{5+} product distribution of catalysts studied after 24 h TOS.

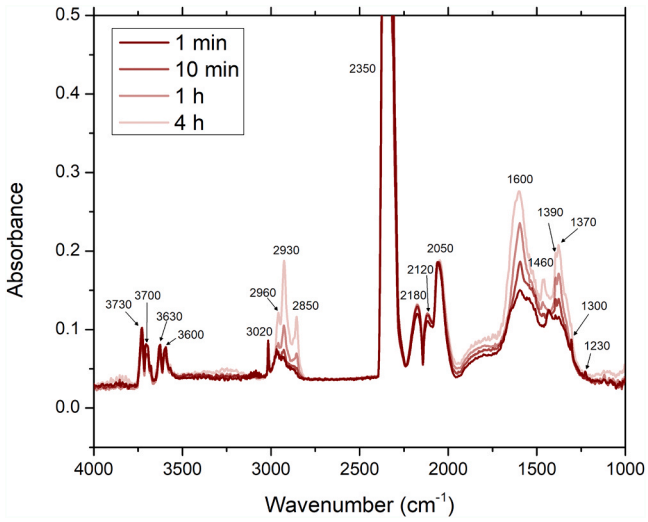

Fig. 9. DRIFTS experiments on CeLa catalyst over time catalyst using 50% H_2/CO – 32.5% CO_2 – 17.5% Ar feed.

The proportion of hydrocarbons (2850–2960 cm^{-1}) in the promoted catalyst was quite similar at equal TOS. Observations on these group bands are more suited for probing early stages of the reaction rather than -CH_x- chain propagation, and thus, to explain the higher selectivity to C_5-C_{20} compounds [45]. Conversely, the oxygenate region presented a different pattern on lanthanide promoted catalysts. The relative size of the band (1460 cm^{-1}), associated to formates and carboxylates, was lower in the promoted catalyst; whereas those of C-H bending (1390 cm^{-1}), OCO stretching (1370 cm^{-1}) were larger, indicating favorable formation of CH_xO complexes. Thus, it is clear that the presence of lanthanides modified the reaction mechanism and thus the selectivity. Mendes et al. [52] suggested that formation of CH_xO species at bimetal interfaces are the precursor of long-chain hydrocarbons. In the present case, the formation of methyl radical groups at interfacial Co^0-CeO_2-La_2O_3 sites may favoured the formation of C_{5+} chains. In any case, further work would be required to confirm this hypothesis.

4. Conclusions

The FTS catalytic performance of the reference micro-catalyst (Co/γ-Al_2O_3, 16.3 wt%) confirmed that the feed composition affected the conversion and the selectivity of the reaction. The replacement of part of syngas by N_2 or CO_2 led to lower catalytic activity because of lower partial pressure of reactants. However, while nitrogen acts as an inert compound, part of carbon dioxide plays a significant role as reactant on

the conversion and the selectivity of FTS. As a result, selectivity towards C_{5+} compounds is enhanced, at the expense of C_1-C_4 fraction. Experimental results were aligned with DRIFTS measurements, which indicated, on the one hand, that the presence of CO_2 in the feed cause the incorporation of the reverse Water Gas Shift reaction into the reaction mechanism and the inhibition of the selectivity to shorter hydrocarbons. On the other hand, that it competes with CO_2 to be adsorbed on the active sites, which lead to lower catalytic activity.

The incorporation of 1 wt% of lanthanides did not practically affect the porosity of the material, but reduced the reducibility and the amount of available cobalt on the surface. Very promising for FTS catalyst development was the fact that selectivity to C_{5+} was highly increased by the presence of lanthanides, without significant differences between lanthanum and cerium oxides. Moreover, lanthanide enhance the selectivity to C_5-C_{18} fraction, in the range of gasoline, kerosene and diesel-type fossil fuels. In this aspect, DRIFTS measurements revealed that the presence of lanthanides under relevant $H_2/CO/CO_2$ mixtures positively affected the reaction mechanism. Conversely, lower reactivity is expected from lanthanide promoted samples due to the lower availability for cobalt active sites. Differences between lanthanum and cerium oxides, or synergetic effects, are clearly discarded.

As an overall, the incorporation of CO_2 on the gas mixture and lanthanides on the catalyst singularly lead to an analogous result. On one hand, the beneficial modification of the reaction mechanism, and thus the selectivity towards interesting liquid fuel fractions. On the other hand, the resulting catalyst is less active, either by CO_2 adsorption or lanthanide deposition on the cobalt active sites, and thus the reactor operation should be carried out at higher gas-catalyst contact times.

CRediT authorship contribution statement

Jordi Guilera: Writing – original draft, Formal analysis, Validation. **José Antonio Díaz-López**: Writing – original draft, Formal analysis, Validation. **Antonio Berenguer**: Conceptualization, Methodology, Investigation, Formal analysis. **Martí Biset-Peiró**: Methodology, Investigation; Writing – review & editing. **Teresa Andreu**: Conceptualization, Methodology, Writing – review & editing, Resources, Supervision.

Declaration of Competing Interest

The authors declare that they have no known competing financial interests or personal relationships that could have appeared to influence the work reported in this paper.

Acknowledgements

This research was funded from the European Union's Horizon 2020 research and innovation program under grant agreement No 764675 (Heat-To-Fuel Project). The authors kindly thank Dan Enache and Gordon Kelly from Johnson Matthey for providing the reference catalyst. Authors kindly thank Dr. Andreina Alarcón and Dr. Albert Llorente from IREC for material characterization.

References

[1] F. Ueckerdt, C. Bauer, A. Dirnaichner, J. Everall, R. Sacchi, G. Luderer, Potential and risks of hydrogen-based e-fuels in climate change mitigation, Nat. Clim. Change 11 (2021) 384–393, https://doi.org/10.1038/s41558-021-01032-7.

[2] C. Panzone, R. Philippe, A. Chappaz, P. Fongarland, A. Bengaouer, Power-to-Liquid catalytic CO_2 valorization into fuels and chemicals: focus on the Fischer-Tropsch route, J. CO2 Util. 38 (2020) 314–347, https://doi.org/10.1016/j.jcou.2020.02.009.

[3] S.S. Ail, S. Dasappa, Biomass to liquid transportation fuel via Fischer Tropsch synthesis – technology review and current scenario, Renew. Sustain. Energy Rev. 58 (2016) 267–286, https://doi.org/10.1016/j.rser.2015.12.143.

[4] E. Sonal, S. Ahmad, K.K.Pant Upadhyayula, Biomass-derived CO_2 rich syngas conversion to higher hydrocarbon via Fischer-Tropsch process over Fe–Co bimetallic catalyst, Int. J. Hydrog. Energy 44 (2019) 27741–27748, https://doi.org/10.1016/j.ijhydene.2019.09.015.

[5] R.G. dos Santos, A.C. Alencar, Biomass-derived syngas production via gasification process and its catalytic conversion into fuels by Fischer Tropsch synthesis: a review, Int. J. Hydrog. Energy 45 (2020) 18114–18132, https://doi.org/10.1016/j.ijhydene.2019.07.133.

[6] S.A. Archer, R. Steinberger-Wilckens, Systematic analysis of biomass derived fuels for fuel cells, Int. J. Hydrog. Energy 43 (2018) 23178–23192, https://doi.org/10.1016/j.ijhydene.2018.10.161.

[7] A.M. Mauerhofer, J. Fuchs, S. Müller, F. Benedikt, J.C. Schmid, H. Hofbauer, CO_2 gasification in a dual fluidized bed reactor system: impact on the product gas composition, Fuel 253 (2019) 1605–1616, https://doi.org/10.1016/j.fuel.2019.04.168.

[8] A.M. Mauerhofer, S. Müller, F. Benedikt, J. Fuchs, A. Bartik, H. Hofbauer, CO_2 gasification of biogenic fuels in a dual fluidized bed reactor system, Biomass Convers. Biorefin. 11 (2021) 1101–1116, https://doi.org/10.1007/s13399-019-00493-3.

[9] W.L. Becker, R.J. Braun, M. Penev, M. Melaina, Production of Fischer-Tropsch liquid fuels from high temperature solid oxide co-electrolysis units, Energy 47 (2012) 99–115, https://doi.org/10.1016/j.energy.2012.08.047.

[10] M. Marchese, E. Giglio, M. Santarelli, A. Lanzini, Energy performance of power-to-Liquid applications integrating biogas upgrading, reverse water gas shift, solid oxide electrolysis and Fischer-Tropsch technologies, Energy Convers. Manag.: X 6 (2020), 100041, https://doi.org/10.1016/j.ecmx.2020.100041.

[11] F. Vidal Vázquez, P. Pfeifer, J. Lehtonen, P. Piermartini, P. Simell, V. Alopaeus, Catalyst screening and kinetic modeling for CO production by high Pressure and temperature reverse water gas shift for Fischer-Tropsch Applications, Ind. Eng. Chem. Res. 56 (2017) 13262–13272, https://doi.org/10.1021/acs.iecr.7b01606.

[12] J.P. Stempien, M. Ni, Q. Sun, S.H. Chan, Thermodynamic analysis of combined solid oxide electrolyzer and Fischer-Tropsch processes, Energy 81 (2015) 682–690, https://doi.org/10.1016/j.energy.2015.01.013.

[13] V. Vakharia, K. Ramasubramanian, W.S. Winston Ho, An experimental and modeling study of CO_2-selective membranes for IGCC syngas purification, J. Memb. Sci. 488 (2015) 56–66, https://doi.org/10.1016/j.memsci.2015.04.007.

[14] L. Peters, A. Hussain, M. Follmann, T. Melin, M.B. Hägg, CO 2 removal from natural gas by employing amine absorption and membrane technology-a technical and economical analysis, Chem. Eng. J. 172 (2011) 952–960, https://doi.org/10.1016/j.cej.2011.07.007.

[15] K.S. Park, K. Saravanan, S.J. Park, Y.J. Lee, K.W. Jeon, J.W. Bae, Effects of CO2on the deactivation behaviors of Co/Al2O3and Co/SiO2in CO hydrogenation to hydrocarbons, Catal. Sci. Technol. 7 (2017) 4079–4091, https://doi.org/10.1039/c7cy01065f.

[16] S.M. Kim, J.W. Bae, Y.J. Lee, K.W. Jun, Effect of CO2in the feed stream on the deactivation of Co/γ-Al2O3 Fischer-Tropsch catalyst, Catal. Commun. 9 (2008) 2269–2273, https://doi.org/10.1016/j.catcom.2008.05.016.

[17] J.A. Díaz, A.R. De La Osa, P. Sánchez, A. Romero, J.L. Valverde, Influence of CO_2 co-feeding on Fischer-Tropsch fuels production over carbon nanofibers supported cobalt catalyst, Catal. Commun. (2014), https://doi.org/10.1016/j.catcom.2013.07.033.

[18] P. Kaiser, R.B. Unde, C. Kern, A. Jess, Production of Liquid Hydrocarbons with CO 2 as carbon source based on reverse water-gas shift and Fischer-Tropsch synthesis, Chemie Ing. Tech. 85 (2013) 489–499, https://doi.org/10.1002/cite.201200179.

[19] P. Kaiser, F. Pöhlmann, A. Jess, Intrinsic and effective kinetics of cobalt-catalyzed Fischer-Tropsch synthesis in view of a power-to-liquid process based on renewable energy, Chem. Eng. Technol. 37 (2014) 964–972, https://doi.org/10.1002/ceat.201300815.

[20] Y.L. Yao, D. Hildebrandt, D. Glasser, X.Y. Liu, Fischer-Tropsch synthesis using H-2/CO/CO_2 syngas mixtures over a cobalt catalyst, Ind. Eng. Chem. Res. 49 (2010) 11061–11066, https://doi.org/10.1021/Ie100414y.

[21] T. Riedel, G. Schaub, K.-W. Jun, K.-W. Lee, Kinetics of CO 2 hydrogenation on a k-promoted Fe catalyst, Ind. Eng. Chem. Res. 40 (2001) 1355–1363, https://doi.org/10.1021/ie000084k.

[22] H.D. Kim, H. Song, A. Fazeli, A. Alizadeh Eslami, Y.S. Noh, N. Ghaffari Saeidabad, K.-Y. Lee, D.J. Moon, CO/CO_2 hydrogenation for the production of lighter hydrocarbons over SAPO-34 modified hybrid FTS catalysts, Catal. Today (2020), https://doi.org/10.1016/j.cattod.2020.06.066.

[23] A.Y. Khodakov, W. Chu, P. Fongarland, Advances in the development of novel cobalt Fischer-Tropsch catalysts for synthesis of long-chain hydrocarbons and clean fuels, Chem. Rev. 107 (2007) 1692–1744, https://doi.org/10.1021/cr050972v.

[24] J.A. Díaz-López, J. Guilera, M. Biset-Peiró, D. Enache, G. Kelly, T. Andreu, Passivation of Co/Al2O3 catalyst by atomic layer deposition to reduce deactivation in the Fischer–Tropsch aynthesis, Catalysts 11 (2021), https://doi.org/10.3390/catal11060732.

[25] H. Karaca, O.V. Safonova, S. Chambrey, P. Fongarland, P. Roussel, A. Griboval-Constant, M. Lacroix, A.Y. Khodakov, Structure and catalytic performance of Pt-promoted alumina-supported cobalt catalysts under realistic conditions of Fischer-Tropsch synthesis, J. Catal. 277 (2011) 14–26, https://doi.org/10.1016/j.jcat.2010.10.007.

[26] M.C. Ribeiro, M.K. Gnanamani, R. Garcia, G. Jacobs, R.C. Rabelo-Neto, F. B. Noronha, I.F. Gomes, B.H. Davis, Tailoring the product selectivity of Co/SiO2 Fischer-Tropsch synthesis catalysts by lanthanide doping, Catal. Today 343 (2020) 80–90, https://doi.org/10.1016/j.cattod.2018.10.064.

[27] F. Bertella, C.W. Lopes, A.C. Foucher, G. Agostini, P. Concepción, E.A. Stach, A. Martínez, Insights into the promotion with Ru of Co/TiO 2 Fischer–Tropsch catalysts: an in situ spectroscopic study, ACS Catal. (2020) 6042–6057, https://doi.org/10.1021/acscatal.9b05359.

[28] H. Romar, E. Rivoire, P. Tynjälä, U. Lassi, Effect of calcination conditions on the dispersion of cobalt over Re, Ru and Rh promoted Co/γ-Al2O3 catalysts, Top. Catal. 60 (2017) 1408–1414, https://doi.org/10.1007/s11244-017-0822-0.
[29] S. Iqbal, T.E. Davies, J.S. Hayward, D.J. Morgan, K. Karim, J.K. Bartley, S. H. Taylor, G.J. Hutchings, Fischer-Tropsch synthesis using promoted cobalt-based catalysts, Catal. Today 272 (2016) 74–79, https://doi.org/10.1016/j.cattod.2016.04.012.
[30] S. Zeng, Y. Du, H. Su, Y. Zhang, Promotion effect of single or mixed rare earths on cobalt-based catalysts for Fischer-Tropsch synthesis, Catal. Commun. 13 (2011) 6–9, https://doi.org/10.1016/j.catcom.2011.06.009.
[31] F. Pardo-Tarifa, S. Cabrera, M. Sanchez-Dominguez, M. Boutonnet, Ce-promoted Co/Al2O3catalysts for Fischer–Tropsch synthesis, Int. J. Hydrog. Energy 42 (2017) 9754–9765, https://doi.org/10.1016/j.ijhydene.2017.01.056.
[32] L. He, B. Teng, Y. Zhang, M. Fan, Development of composited rare-earth promoted cobalt-based Fischer-Tropsch synthesis catalysts with high activity and selectivity, Appl. Catal. A Gen. 505 (2015) 276–283, https://doi.org/10.1016/j.apcata.2015.07.041.
[33] C. Ochoa-Hernández, Y. Yang, P. Pizarro, V.A. de la Peña O'Shea, J.M. Coronado, D.P. Serrano, Hydrocarbons production through hydrotreating of methyl esters over Ni and Co supported on SBA-15 and Al-SBA-15, Catal. Today 210 (2013) 81–88, https://doi.org/10.1016/j.cattod.2012.12.002.
[34] A. Alarcón, J. Guilera, J.A. Díaz, T. Andreu, Optimization of nickel and ceria catalyst content for synthetic natural gas production through CO<inf>2</inf> methanation, Fuel Process. Technol. 193 (2019), https://doi.org/10.1016/j.fuproc.2019.05.008.
[35] J. Guilera, J. del Valle, A. Alarcón, J.A. Díaz, T. Andreu, Metal-oxide promoted Ni/Al2O3 as CO_2 methanation micro-size catalysts, J. CO2 Util. 30 (2019) 11–17, https://doi.org/10.1016/j.jcou.2019.01.003.
[36] Y. Zhang, K. Liew, J. Li, X. Zhan, Fischer-Tropsch synthesis on lanthanum promoted Co/TiO2, Catal. Lett. 139 (2010) 1–6, https://doi.org/10.1007/s10562-010-0407-z.
[37] M. Mehrbod, M. Martinelli, J.D. Castro, N. Alhraki, D.C. Cronauer, A.J. Kropf, C. L. Marshall, G. Jacobs, Fischer-Tropsch synthesis: direct cobalt nitrate reduction of promoted Co/Al2O3 catalysts, Catal. Today 369 (2021) 129–143, https://doi.org/10.1016/j.cattod.2020.03.033.
[38] J. Clarkson, P.R. Ellis, R. Humble, G.J. Kelly, M. McKenna, J. West, Deactivation of alumina supported cobalt FT catalysts during testing in a continuous-stirred tank reactor (CSTR), Appl. Catal. A Gen. 550 (2018) 28–37, https://doi.org/10.1016/j.apcata.2017.10.014.
[39] G. Jacobs, T.K. Das, Y. Zhang, J. Li, G. Racoillet, B.H. Davis, Fischer–Tropsch synthesis: support, loading, and promoter effects on the reducibility of cobalt catalysts, Appl. Catal. A Gen. 233 (2002) 263–281, https://doi.org/10.1016/S0926-860X(02)00195-3.
[40] D.J. Moodley, A.M. Saib, J. Van De Loosdrecht, C.A. Welker-Nieuwoudt, B. H. Sigwebela, J.W. Niemantsverdriet, The impact of cobalt aluminate formation on the deactivation of cobalt-based Fischer-Tropsch synthesis catalysts, Catal. Today 171 (2011) 192–200, https://doi.org/10.1016/j.cattod.2011.03.078.
[41] A. Carrero, A.J. Vizcaíno, J.A. Calles, L. García-Moreno, Hydrogen production through glycerol steam reforming using Co catalysts supported on SBA-15 doped with Zr, Ce and La, J. Energy Chem. 26 (2017) 42–48, https://doi.org/10.1016/j.jechem.2016.09.001.
[42] J. Lu, X. Li, S. He, C. Han, G. Wan, Y. Lei, R. Chen, P. Liu, K. Chen, L. Zhang, Y. Luo, Hydrogen production via methanol steam reforming over Ni-based catalysts: influences of lanthanum (La) addition and supports, Int. J. Hydrog. Energy 42 (2017) 3647–3657, https://doi.org/10.1016/j.ijhydene.2016.08.165.
[43] H. Schulz, E. van Steen, M. Claeys, Specific inhibition as the kinetic principle of the Fischer-Tropsch synthesis, Top. Catal. 2 (1995) 223–234, https://doi.org/10.1007/BF01491969.
[44] D. Tristantini, S. Lögdberg, B. Gevert, Ø. Borg, A. Holmen, The effect of synthesis gas composition on the Fischer–Tropsch synthesis over Co/γ-Al2O3 and Co–Re/γ-Al2O3 catalysts, Fuel Process. Technol. 88 (2007) 643–649, https://doi.org/10.1016/j.fuproc.2007.01.012.
[45] M. Kollár, A. De Stefanis, H.E. Solt, M.R. Mihályi, J. Valyon, A.A.G. Tomlinson, The mechanism of the Fischer-Tropsch reaction over supported cobalt catalysts, J. Mol. Catal. A Chem. 333 (2010) 37–45, https://doi.org/10.1016/j.molcata.2010.09.014.
[46] B. Liang, H. Duan, X. Su, X. Chen, Y. Huang, X. Chen, J.J. Delgado, T. Zhang, Promoting role of potassium in the reverse water gas shift reaction on Pt/mullite catalyst, Catal. Today 281 (2017) 319–326, https://doi.org/10.1016/j.cattod.2016.02.051.
[47] J.A. Hernandez Lalinde, P. Roongruangsree, J. Ilsemann, M. Bäumer, J. Kopyscinski, CO_2 methanation and reverse water gas shift reaction. Kinetic study based on in situ spatially-resolved measurements, Chem. Eng. J. 390 (2020), 124629, https://doi.org/10.1016/j.cej.2020.124629.
[48] A. Goguet, F.C. Meunier, D. Tibiletti, J.P. Breen, R. Burch, Spectrokinetic investigation of reverse water-gas-shift reaction intermediates over a Pt/CeO2 catalyst, J. Phys. Chem. B 108 (2004) 20240–20246, https://doi.org/10.1021/jp047242w.
[49] S. Eckle, H.-G. Anfang, R.J. Behm, Reaction intermediates and side products in the methanation of CO and CO_2 over supported Ru catalysts in H2-rich reformate gases, J. Phys. Chem. C 115 (2011) 1361–1367, https://doi.org/10.1021/jp108106t.
[50] Y.A. Daza, J.N. Kuhn, CO_2 conversion by reverse water gas shift catalysis: comparison of catalysts{,} mechanisms and their consequences for CO_2 conversion to liquid fuels, RSC Adv. 6 (2016) 49675–49691, https://doi.org/10.1039/C6RA05414E.
[51] M.K. Gnanamani, W.D. Shafer, D.E. Sparks, B.H. Davis, Fischer-Tropsch synthesis: effect of CO_2 containing syngas over Pt promoted Co/γ-Al2O3 and k-promoted Fe catalysts, Catal. Commun. 12 (2011) 936–939, https://doi.org/10.1016/j.catcom.2011.03.002.
[52] F.M.T. Mendes, C.A.C. Perez, F.B. Noronha, C.D.D. Souza, D.V. Cesar, H.J. Freund, M. Schmal, Fischer-Tropsch synthesis on anchored Co/Nb2O5/Al2O3 catalysts: the nature of the surface and the effect on chain growth, J. Phys. Chem. B 110 (2006) 9155–9163, https://doi.org/10.1021/jp060175g.